One pot synthesis of amino functionalized mesoporous silica materials: using simulations to understand transitions between different structures

Alessandro Patti,[†] Allan D. Mackie,[‡] Vladimir Zelenak[§] and Flor R. Siperstein[¶]

[†]Soft Condensed Matter, Debye Institute for Nanomaterials Science, Utrecht University, Princetonplein 5, Utrecht 3584 CC, The Netherlands

[‡]Departament d'Enginyeria Química, Universitat Rovira i Virgili, Av. Països Catalans, 26 Tarragona 43007, Spain.

[§]Department of Inorganic Chemistry, Faculty of Science, P. J. Safarik University, SK-041 54 Kosice, Slovak Republic.

[¶]School of Chemical Engineering and Analytical Science, University of Manchester, Manchester M60 1QD, UK

Abstract

The rich phase behavior of surfactants can be exploited to design materials with a given desired structure and properties. One example includes aminofunctionalized mesoporous silicas, which can be used in different environmental applications, including removal of heavy metals from water and CO_2 separation and purification. These applications may require a high concentration of functional groups, but the increased concentration of hybrid organic-inorganic precursors can lead to the destruction of the liquid crystals or transformation into other phases. In this work, we modeled the phase behavior of such systems using lattice Monte Carlo simulations and analyzed the distribution of hybrid organic-inorganic precursors to explain the observed changes in the liquid crystal structures. In particular, we observed that if the hybrid precursor is sufficiently hydrophobic, it can act as a cosurfactant, swell the core of the surfactant liquid crystal, and lead to structures with smaller interfacial curvature. On the other hand, if the hybrid precursor acts as a cosolvent it will solubilise the surfactant leading to the destruction of the preformed liquid crystal.

Introduction

Over the past two decades, researchers have made significant progress towards designing novel mesostructured inorganic-organic hybrids and the associated porous mesostructured inorganic frameworks.[1-11] These materials were first synthesized by mixing a micellar solution of CTAB (cetyl trimethyl ammonium bromide) with TEOS (tetraethyl orthosilicate) under basic conditions.[12,13] Soon after, the synthesis protocol was extended to acid conditions[14,15] and a variety of amphiphilic molecules, including nonionic surfactants[16] and block copolymers.[17] Mesostructured organic-inorganic hybrids are not restricted to silica based materials. Well ordered materials can be obtained using a variety of sources, including transition metal oxides[18], non oxidic materials[19] and hybrid organic-inorganic precursors[20-22]. The use of hybrid precursors has attracted the attention of the scientific community because the presence of functional groups can be important in sorption and release of bioactive molecules,[23-25] purifications,[26-33] analytic[34,35] and optical[36,37] applications. In particular, it has been suggested that functionalizing mesoporous materials with amine groups can be useful for CO_2 capture and separations.[38-52]

The addition of functional groups to periodic mesoporous organosilicas (PMOs) can be accomplished by two main routes: (1) one pot condensation of an organosilane around a soft organic template, or (2) grafting of organosilanes after the PMO has been obtained. Both methods have advantages and disadvantages, which are extensively discussed in recent reviews.[11,53] In general, well ordered materials are not obtained in a one pot synthesis when using terminal organosilica precursors, of the form $(EtO)_3–Si–R$, but high quality materials can be obtained using bridging organosilica precursors, of the form $(EtO)_3–Si–R–Si–(EtO)_3$.

Terminal organosilica precursors often lead to the formation of poorly ordered PMOs, but mixing terminal organosilica precursors with silica precursors can lead to the formation of well ordered PMOs. Nevertheless, the location of the organic groups and the possible segregation of the different precursors can lead to an inhomogeneous material. This problem is not exclusive to the formation of PMOs using terminal organosilica precursors, but can also be found when mixing different bridging organosilica precursors. Recently, researchers have been interested in synthesizing materials with multiple functionalities and identifying the relative location of the organic groups.[54,55] In this work, we are interested in understanding the changes in the liquid crystal structures when using a variety of amino functionalized precursors mixed with a silica precursor (TEOS) in a co-condensation synthesis.

Co-condensation and post synthesis of mesoporous materials functionalized with amines groups has been explored for several precursors.[21,39,56,57] Amine functionalized materials are of interest for CO_2 capture and separations as well as for removal of heavy metals from aqueous solutions. Co-condensation of hybrid precursors, aminopropyl-trimethoxysilane (AP), aminoethyl-aminopropyl-trimethoxysilane (DAP) or trimethoxysilyl-propyl-diethylentriamine (TAP), with tetraethyl orthosilicate (TEOS) leads to a uniform distribution of amine groups in the material framework. Nevertheless, hexagonally ordered materials were only obtained at small ratios of hybrid precursor to TEOS. As the concentration of hybrid precursor increased, the XRD patterns of the resulting material showed only a single broad peak, indicating the pores were no longer ordered in an hexagonal arrangement.[39] Zelenak and coworkers have recently shown that increasing the ratio of phenyl-3-aminoproyltrimethoxysilane (PAP) to TEOS can lead to the formation of lamellar structures while the use of methyl-3-aminopropyl-trimethoxysilane (MAP) destroys the liquid crystal order as in the case of AP.[58]

With this work, we propose that the destruction of the hexagonal phase when increasing the concentration of AP and MAP is a consequence of the difference in the solvent quality when adding the hybrid precursor, while the formation of a lamellar phase when increasing the concentration of PAP is due to the swelling of the hydrophobic region of the cylindrical micelles. We propose

that the methods used in this work can be applicable to a variety of systems to identify regions in the phase diagram where materials with desirable properties can be obtained. Alternatively, one can map which type of precursor is likely to maintain, destroy or transform ordered liquid crystal phases. In addition, these simulations provide direct information with respect to the segregation or mixing of different precursors in the synthesis of multifunctional materials, where the synthesis is not kinetically controlled.

We model the structures of PMOs obtained through the condensation of organosilica precursors in the presence of surfactants, under the assumption that the structures obtained experimentally reach thermodynamic equilibrium. A discussion on the different kinetic processes and their importance in the formation of ordered mesoporous materials can be found elsewhere.[59] Previous work[60] shows that this assumption is valid when results are compared to the behavior observed experimentally of silica surfactant liquid crystals.[61] Similar approaches have been used to model the structure of mesocellular foams[62] and hybrid organic-inorganic materials.[63,64] We have shown that the nature of the organic functional group has an important influence on the range of structures obtained: a solvophilic functional group will be more likely to form ordered structures, whereas a solvophobic functional group acts as a good solvent for the surfactant preventing the microphase separation in the surfactant rich phase.[63,64] We have selected to use a simple model to describe the different components in the system because modeling fully atomistic systems would be impossible for practical purposes given the size of systems needed. Currently, fully atomistic dynamic simulations to model the formation of mesoporous materials is restricted to the very early stages of the synthesis and to a relatively small number of surfactant chains[65] or is focused exclusively on the silica condensation.[66-70]

In the remaining of this paper we describe the model and simulation methods used, followed by an analysis of the results that lead us to the conclusion that the changes in the original liquid crystal are due to the changes in solvent quality or cosurfactant behavior of the hybrid precursor.

Model and simulation methodology

In order to observe the formation of ordered mesoporous structures, we used the coarse-grained lattice model and simulation methodology already discussed in previous works, where a system containing a diblock copolymer, a hybrid or a pure silica precursor, and a solvent, was studied.[63,64] In the following, we review their main features including some differences concerning the architecture of the components, and refer the reader to the references for more details.[63,64] The system is composed of four components: a surfactant, a pure silica precursor, a hybrid precursor, and a solvent, being arranged in a fully occupied three dimensional lattice box. The surfactant, T_5HH_3, is made up of a linear tail of five segments *T*, and a bulky head, that hereinafter will be called a branched head, composed of four segments *H*, disposed as illustrated in Figure 1. The structure of this surfactant creates a large solvophilic cross-sectional area and favors the formation of spherical micelles and cylindrical aggregates in comparison with a linear surfactant of the same composition.

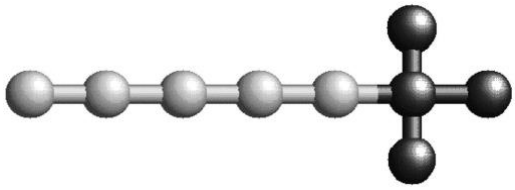

Fig. 1. Model surfactant T_5HH_3. Dark and light shading represent the surfactant head and tail, respectively.

The tail segments constitute the solvophobic part of the amphiphilic chain, whereas the head segments constitute the solvophilic section. It should be noted that the branched head sites interact with the neighboring sites in the same way as any other head segment. A linear surfactant (or copolymer) can be considered a model structure directing agent for the synthesis of SBA-15-like mesoporous materials, whose mesopores are generally interconnected by micropores. In contrast, the branched-head surfactants are useful to model the self-assembling of MCM-41-like materials, where the mesopores are not interconnected and the wall thickness can be significantly thinner, and more importantly, the wall thickness to pore diameter should be small.[17] Moreover, the branched head can more realistically represent the large head of actual surfactants used experimentally, such as cetyl trimethylammonium bromide (CTAB), which is one of the most common structure directing agents used in the synthesis of MCM-41.[12] In a continuum model this can be accomplished by changing the size of the head group, which would be more complicated to do in a lattice model.

The silica precursor generally used in the synthesis of mesoporous materials (TEOS) was modeled by a chain of two soluble beads, I_2, forming strong interactions with the surfactant head. The hybrid precursors can be of different kinds, according to the functionality to be given to the mesopores. In this work, we are interested in primary or secondary amines of the type given in Figure 2.

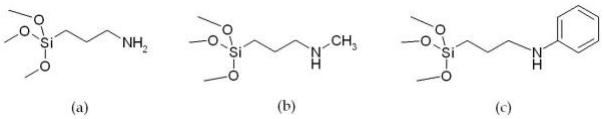

Fig. 2. Amine-modified TEOSs used in the synthesis of MCM-41: (a) aminopropyl-trimethoxysilane (AP), (b) methyl-3-aminopropyltrimethoxysilane (MAP), and phenyl-3-aminoproyltrimethoxysilane (PAP).

Such amine-modified TEOSs were modeled by adding to I_2 a given number of segments reproducing the solvophobic nature of the organic substituents. In particular, we modeled the propyl chain by one single *T* segment; the methyl and aromatic group of the secondary amines by one and three *T* segments, respectively; and the NH or NH_2 group by a single *H* segment. We made *T* (*H*) segments as solvophobic (solvophilic) as the surfactant tail (head) segments. Therefore, the primary amine was modeled by the linear chain I_2TH, the secondary amine with a methyl substituent by I_2THT, and the aromatic amine with I_2THT_3. They are given in Figure 3 along with the model pure silica precursor.

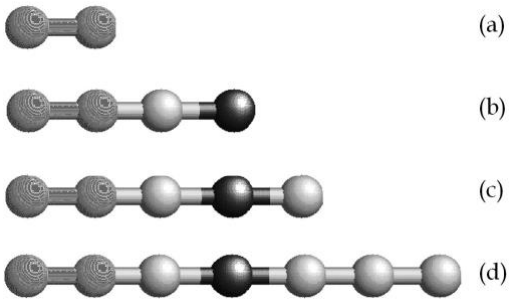

Fig. 3. Model precursors: (a) I_2, (b) I_2TH, (c) I_2THT, and (d) I_2THT_3, which represent TEOS, AP, MAP and PAP respectively.

From now on, we will refer to the set of *T* and *H* segments directly linked to I_2 as the functional group of the hybrid precursors. We identify the *T* segment directly connected to I_2 as T_α.

The solvent beads occupying single empty sites in the lattice box are denoted by *S*. The solvent is not explicitly modeled and the surfactant heads are completely miscible with it. All segments lie on a cubic lattice whose coordination number is 26. The global interchange energy between pairs of sites reads:

$$\omega_{ij} = \varepsilon_{ij} - \frac{1}{2}\left(\varepsilon_{ii} + \varepsilon_{jj}\right) \quad (1)$$

with $i \neq j$ and ε_{ij} being the individual interaction energies of a given pair of sites. The values of these interactions, reported elsewhere,[63,64] are applied for the hybrid precursors, whose *I*, *T*, and *H* beads interact as those in the pure silica precursor chain or in the surfactant chain.

The dimensionless temperature reads

$$T^* = k_B T / \omega_{HT} \quad (2)$$

where k_B is the Boltzmann constant, *T* is the absolute temperature, and ω_{HT} is the surfactant head-tail interaction energy. All simulations have been performed at the reduced temperature T^*=8.0.

To make the system evolve from a completely random initial configuration to an ordered configuration, Monte Carlo simulations in the *NVT* ensemble have been performed in an elongated box of volume 24×24×100 or in a cubic box of volume 40×40×40. The elongated box was used to analyze the phase separation between a surfactant-rich phase and a solvent-rich phase, and the cubic box to study the structure of the ordered phases obtained. In both cases, periodic boundary conditions have been applied. All the chains have been displaced by configurational bias moves, namely by partial regrowth and complete regrowth[72]. The linear chains were also moved by reptation, where a randomly selected chain end can be displaced to a neighboring site occupied by the solvent, according to the Metropolis algorithm[72].

A typical mix of the MC moves used was 15% reptation, 20% complete regrowth and 65% partial regrowth. Since we do not move the surfactant chains by reptation, we increased the probability to select these chains for a bias move with respect to the precursor chains. In particular, 90% of the attempted bias moves are performed on surfactant chains and the remaining 10% on the others.

In order to evaluate the distribution of the functional group of the hybrid precursors inside the pores of the material, we calculated the radial density profiles, $\rho_j(r)$, giving the composition of a certain segment *j* around the axes of the self-assembled cylinders[63]. In particular, we compared the density profiles of the functional group of the hybrid precursors with those of the pure silica precursor I_2, to establish the position of the functional groups with respect to the inorganic pore walls. When lamellar structures are formed, a plane at the centre of the solvophobic segments of a given layer was identified, and the composition profile was obtained in the direction normal to the plane.

The inorganic wall thickness is calculated by considering the segments of type *I* of the pure silica and hybrid precursors, and is defined as the distance between the first two points in their normalized density distribution profile, whose value is 1. Such a definition, being completely arbitrary, considers as wall thickness that part of the material surrounding the pore where most of the inorganic moiety is concentrated.

Results

In this section, we first report a brief analysis of the phase and aggregation behavior of the binary T_5HH_3/S and ternary T_5HH_3/I_2/S systems, and then we discuss the results obtained in the four component system containing a hybrid precursor.

Binary mixtures of the surfactant T_5HH_3 with the solvent *S* form hexagonal phases at concentrations between 50% and 70% by volume and T^*=8.0. At higher concentrations, lamellar phases have been observed (see Figure 4). Therefore, the temperature of the order-disorder transition must be higher than T^*=8.0 for this specific surfactant in solution.

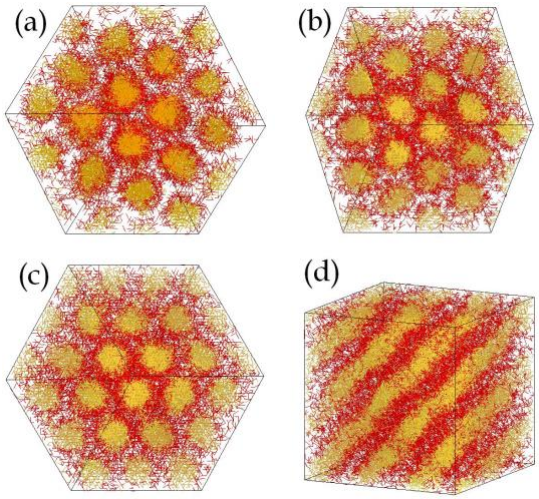

Fig. 4. Hexagonal and lamellar phases obtained at T^*=8.0 in binary systems T_5HH_3/S. Surfactant volume fractions: 50% (a), 58% (b), 70% (c), and 75% (d). The yellow and red segments represent the surfactant tails and heads, respectively. The solvent is not shown. MC steps: 60×10^9. Box volume: 40×40×40.

When small concentrations of the pure silica precursor I_2 were added to this binary system, we obtained hexagonally ordered liquid crystal phases as a result of the phase separation between a solvent rich-phase and a surfactant-rich phase containing approximately between 50% and 65% of surfactant, and between 10% and 30% of pure silica precursor. Such a phase separation is driven by the strong attraction between the surfactant heads and the inorganic

precursor. In Figure 5, the ternary phase diagram of the $T_5HH_3/I_2/S$ system at T^*=8.0 is given.

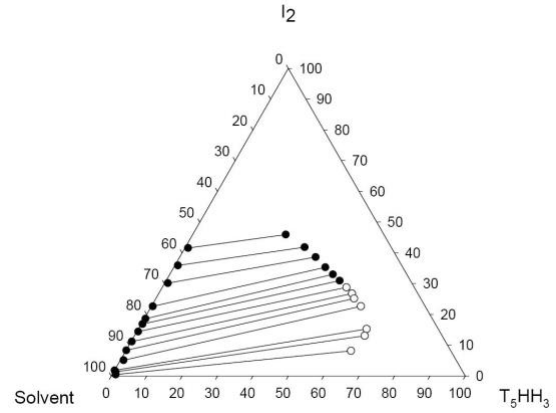

Fig. 5. Ternary phase diagram of the system $T_5HH_3/I_2/S$ obtained by MC simulations at T^*=8.0. The blank and black circles indicate the presence of hexagonally ordered phases and weakly ordered phases, respectively.

Such a diagram is very similar to that calculated for the ternary system containing the linear surfactant chain H_4T_4 and the same precursor and solvent[63,64], although in this case the immiscibility gap is slightly bigger because the driving force for the phase separation is increased by the lower solubility of T_5HH_3 in the solvent-rich phase. The slight difference in the solubility can be attributed to the solvophobic tail of T_5HH_3 being longer than that of H_4T_4.
A typical configuration, obtained after 80×10^9 MC steps, of a system with 50% surfactant and 10% pure silica precursor is shown in Figure 6. The final surfactant-rich phase contains approximately 65% surfactant, being usually more than enough to observe the formation of a hexagonal phase.

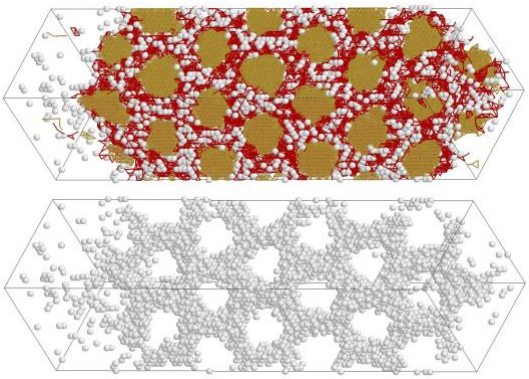

Fig. 6. Phase separation observed in the system $T_5HH_3/I_2/S$ at T^*=8.0 in a lattice box of volume 24×24×100. Global concentrations: 50% T_5HH_3, 10% I_2. The yellow segments represent the surfactant tails, the red segments represent the surfactant heads, and the white spheres represent the inorganic precursor. The solvent is not shown. In the bottom figure, the surfactant is not shown.

To study the phase behavior of amphiphilic systems containing pure silica and a hybrid precursor, we added amine-modified TEOSs of the types given in Figure 3. I_2TH and I_2THT are completely soluble in the solvent, whereas I_2THT_3 is only partially soluble and its limit of solubility at T^*=8.0 is 3%. By looking at the ternary phase diagram $T_5HH_3/I_2/S$ in Figure 5, we can see that periodic hexagonally-ordered phases are formed at a surfactant concentration of 50%, with pure silica precursor varying approximately between 10% and 30%. Therefore, in the systems with four components, we decided to verify the possible formation of hexagonally ordered phases by decreasing the percentage of I_2 and gradually adding the hybrid precursors. As a general result, we observed phase separation between a solvent-rich phase, almost completely formed by the solvent and a given amount of the soluble precursors, and a surfactant-rich phase where hexagonally ordered structures were detected.
Tables 1-3 contain the volume fractions of the surfactant-rich and solvent-rich phases for the systems containing I_2TH, I_2THT, and I_2THT_3, respectively.
The surfactant rich phase has cylinders in a hexagonal arrangement for low concentrations of hybrid precursors, which are destroyed or transformed into lamellar structures as the concentration of hybrid precursors increases.

Table 1. Volume fraction in the systems containing I_2TH. H, L, and D stand for hexagonal, lamellar, and very weakly ordered phases, respectively. Global surfactant concentration: 40%.

Global Conc. (%)		Surfactant-rich phase (%)				Solvent-rich phase (%)		
I_2	I_2TH	T_5HH_3	I_2	I_2TH	Order	T_5HH_3	I_2	I_2TH
19.0	1.0	56.8	23.1	1.3	H	0.5	8.0	0.6
18.0	2.0	57.2	22.5	2.1	H	0.2	7.7	0.7
17.0	3.0	57.7	21.4	3.2	H	0.4	6.3	1.7
16.0	4.0	57.0	20.2	4.7	H	0.4	6.4	1.9
15.0	5.0	56.1	19.0	6.0	H	0.1	5.5	2.6
10.0	10.0	54.0	12.8	11.8	H	0.4	2.5	3.7
10.0	13.0	50.8	11.9	14.6	H	0.2	2.9	4.5
10.0	15.0	48.4	11.4	16.1	D	1.2	3.6	7.1

Table 2. Volume fraction in the systems containing I_2THT. H, L, and D stand for hexagonal, lamellar, and very weakly ordered phases, respectively. Global surfactant concentration: 40%.

Global Conc. (%)		Surfactant-rich phase (%)				Solvent-rich phase (%)		
I_2	I_2THT	T_5HH_3	I_2	I_2THT	Order	T_5HH_3	I_2	I_2THT
19.0	1.0	56.9	23.4	1.3	H	0.1	7.7	0.6
18.0	2.0	56.3	22.7	2.4	H	0.9	7.1	0.8
17.0	3.0	56.7	21.4	3.8	H	0.1	5.7	1.1
16.0	4.0	56.3	19.7	4.9	H	0.3	6.0	1.4
15.0	5.0	56.3	18.9	6.0	H	0.3	5.3	1.9
10.0	10.0	55.0	12.8	12.5	H	0.4	3.1	2.8
10.0	15.0	49.7	11.6	17.2	H	1.7	3.6	5.5
10.0	20.0	46.8	11.0	21.4	H	2.9	4.6	10.7
10.0	25.0	40.0	10.0	25.0	D	one phase		

Table 3. Volume fraction in the systems containing I_2THT_3. H, L, and D stand for hexagonal, lamellar, and very weakly ordered phases, respectively. Global surfactant concentration: 40%.

Global Conc. (%)		Surfactant-rich phase (%)				Solvent-rich phase (%)		
I_2	I_2THT_3	T_5HH_3	I_2	I_2THT_3	Order	T_5HH_3	I_2	I_2THT_3
19.0	1.0	58.1	23.9	1.5	H	0.3	7.7	0.0
18.0	2.0	56.6	22.6	2.6	H	0.7	7.2	0.1
17.0	3.0	56.9	21.6	4.2	H	0.3	6.2	0.1
16.0	4.0	56.7	20.1	5.5	H	0.3	5.9	0.0
15.0	5.0	55.7	19.0	7.0	H	0.0	4.7	0.3
10.0	10.0	54.9	13.0	13.3	H	0.2	2.6	0.2
10.0	15.0	50.9	11.9	19.1	H	0.5	3.0	0.4
10.0	18.0	50.3	11.7	23.0	L	0.8	3.0	0.6
10.0	20.0	49.2	11.4	23.5	L	0.8	3.7	0.5
10.0	25.0	46.0	10.8	28.3	L	1.2	4.2	1.0

Several images obtained during the simulations showing the phase separation between a solvent-rich phase and a surfactant-rich phase are given in Figure 7. The driving force for the phase separation is still due to the strong attraction between the inorganic segments and the surfactant heads. The repulsion between the inorganic segments and the surfactant tails affects the location of the inorganic precursor around the cylindrical aggregates. Because of the low solubility of I_2THT_3 in the solvent, most of the hybrid

precursors are incorporated in the framework, whereas some of the more soluble hybrid precursors are present in the solvent rich phase.

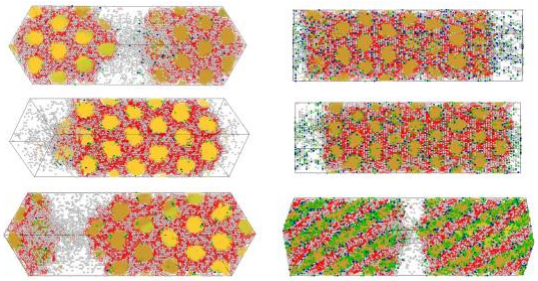

Fig. 7. Phase separation observed at T^*=8.0 in lattice boxes of volume 24×24×100. Global concentrations: 40% T_5HH_3 – 19% I_2 – 1% I_2TH (top left), 40% T_5HH_3 – 10% I_2 – 10% I_2TH (top right); 40% T_5HH_3 – 19% I_2 – 1% I_2THT (centre left), 40% T_5HH_3 – 10% I_2 – 15% I_2THT (centre right), 40% T_5HH_3 – 19% I_2 – 1% I_2THT_3 (bottom left), and 40% T_5HH_3 – 10% I_2 – 25% I_2THT_3 (bottom right). Surfactant heads and tails are shown in red and yellow, respectively; the inorganic group of the precursor in gray; H and T segments of the hybrid precursors are shown in blue and green, respectively. The solvent is not shown.

At 10% of I_2, the highest concentrations at which hexagonal phases have been observed are 13% for I_2TH, 20% for I_2THT, and 15% for I_2THT_3. In particular, in systems with I_2TH or I_2THT, no other ordered phases have been noticed, whereas in those containing between 18% and 25% of I_2THT_3, we detected lamellar phases in equilibrium with a very dilute solvent-rich phase. In this case, the surfactant concentration in the ordered phase is slightly less than 50%, being much lower than that needed for the formation of lamellar phases in binary T_5HH_3/S systems (see Figure 4). We propose that the hybrid precursor I_2THT_3 swells the solvophobic regions created by the surfactant in the formation of the ordered structures and causes the transition to lamellar phases as observed experimentally with long-chain amines or alcohols[73]. For this reason, the behavior of I_2THT_3 can be regarded as that typical of a cosurfactant.

In order to study the distribution of the precursors and, in general, the morphology of the ordered structures, we calculated the concentrations of the four components in the concentrated phase and then we isolated and simulated this phase in cubic boxes of volume 40^3, as indicated in Figure 8.

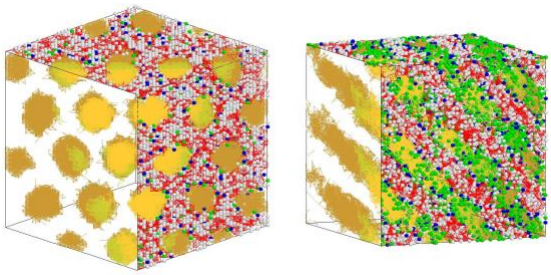

Fig. 8. Representative hexagonal and lamellar structures obtained during the simulations of systems with I_2TH (left) and I_2THT_3 (right) at T^*=8.0 in lattice boxes of volume 40^3. Surfactant heads and tails are shown in red and yellow, respectively; the inorganic part of the precursors in gray; H and T segments belonging to the hybrid precursor are shown in blue and green, respectively. Concentrations: 56.1% T_5HH_3 – 19.0% I_2 – 6.0% I_2TH (left), and 46.0% T_5HH_3 – 28.3% I_2 – 10.8% I_2THT_3 (right). The solvent is not shown. Parts of the system show only the surfactant tails to better appreciate the structural order.

The penetration of the terminal T_3 belonging to I_2THT_3 in the lamellar structures can be seen in Figure 9, where the composition profile perpendicular to the lamellar layers is shown. While T_α and H from the hybrid precursor are retained practically at the interface between the solvophobic and solvophilic regions, all inorganic segments are located in the solvophilic region, and the terminal T_3 from the hybrid precursor are located in the solvophobic regions.

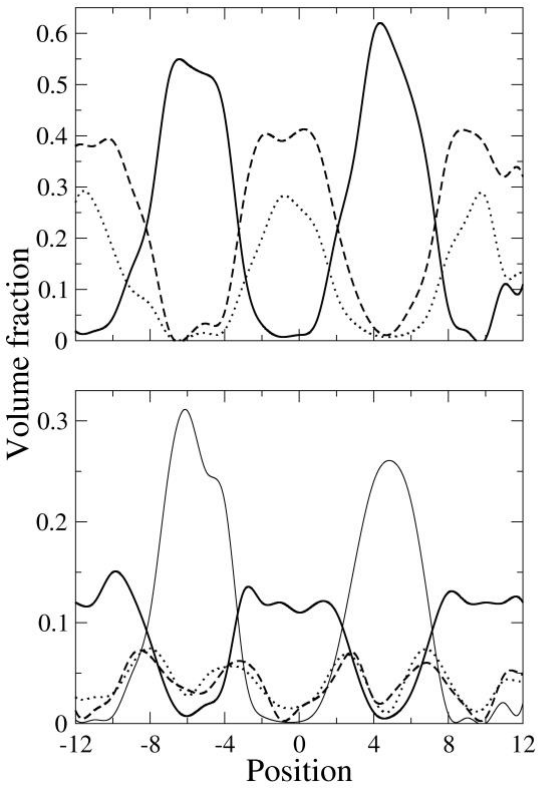

Fig. 9. Composition profile in lamellar structures obtained at high concentrations of PAP. Top graph: the solid line represents the surfactant tail, the dashed line the surfactant head, and the dotted the inorganic precursor. Bottom graph: the solid line represents the inorganic part of the hybrid precursor, the dotted line the amine group (H in the hybrid precursor), the dashed line $T_{\square}$ and the thin solid line T_3 in the hybrid precursor.

By a simple visual inspection of the hexagonal-packed structures, it is possible to see that the functional group of the hybrid precursor is mainly located around the corona of the cylindrical aggregates. However, to properly quantify the distribution of this group with respect to the template and inorganic framework, for the three hybrid precursors modeled, we calculated the normalized density profiles. The normalized density profile of segments of type j, $\rho_{j,N}(r)$, is defined as the ratio between the composition profile $\rho_j(r)$ at a given distance r from that segment and the global composition in the box, ρ_j. By definition, $\rho_{j,N}(r)$ should converge to 1 at large values of r.

In Figure 10, we show the normalized density profiles of the inorganic segments belonging to both the pure silica and hybrid precursor, $\rho_{I,N}$, and representing the inorganic framework of the mesoporous structure. The concentration

of the inorganic segments in the core of the cylindrical aggregates is negligible, and reaches its maximum in the space between neighboring cylinders. Such a region, where the segments of type I belonging to both the inorganic precursors mainly accumulate, represents the thickness of the pore walls, which is arbitrarily defined here as the distance between the first two points where $\rho_{j,N}(r) = 1$. For the systems reported in Figure 10 the wall thickness is approximately equal to 5 lattice units.

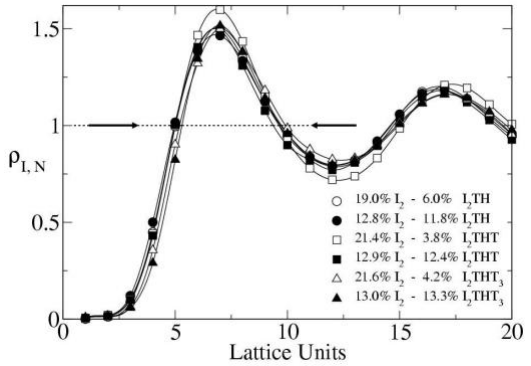

Fig. 10. Normalized density profiles in hexagonally-packed phases of the inorganic beads, I, in the systems indicated in the legend. The arrows define the thickness of the inorganic pore walls. The surfactant concentration is between 54% and 57% by volume (see Tables 1, 2, and 3).

This result is general for all the systems studied here and leads to the conclusion that the thickness of the pore walls does not depend on the type or concentration of the model OSP. However, according to the experiments of Pinnavaia and Mori[74], the solvophobic interactions established between the terminal organic moiety of the OSP and the surfactant tails constrain the molecules of the OSP to stay as close as possible to the core of the cylindrical aggregates. When such attractive interactions become strong enough, they might even cause the mesopores to shrink. The amine-modified TEOS of the type given in figure 2 contain a solvophilic group reducing, and sometimes compensating, this effect. As a result, increasing the concentration of a given OSP whose terminal chain is not too solvophobic, can affect the distribution of the inorganic framework around the template and, as observed experimentally with several types of cosurfactants[73], can lead to the swelling of the pore[39]. The overall effect, being a compromise between the swelling action of the solvophilic amine group, H, and the shrinking action of the terminal T_α group, seems to be neglible with the precursors modeled in this work, whose $\rho_{I,N}(r)$ in the core of the cylindrical aggregates does not show any significant change when their concentration is increased.

The transition from the hexagonal to the lamellar phase observed with the I_2THT_3, swelling the solvophobic core of the cylindrical aggregates, is more likely due to its role as cosurfactant than to the dominating effect of the solvophilic amine group, H, over the terminal T_α group.

By comparing the normalized density profiles of the inorganic segments, $\rho_{I,N}(r)$, and those of the surfactant heads, $\rho_{H,N}(r)$, we observe that the first peak of $\rho_{H,N}(r)$ is broader and slightly smaller than that of $\rho_{I,N}(r)$ (see Figure 11). Therefore, the inorganic segments do not penetrate very much into the corona of the cylindrical aggregates, but prefer to accumulate approximately at a medium distance between neighboring cylinders.

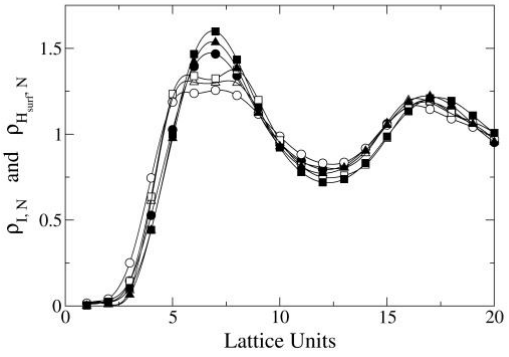

Fig. 11. Normalized density profiles of the inorganic segments belonging to the precursors (solid symbols) and of the surfactant heads (blank symbols) in hexagonally-packed phases. Concentrations: 12.8% I_2 – 11.8% I_2TH (circles), 21.4% I_2 – 3.8 I_2THT (squares), 23.6% I_2 – 1.4% I_2THT_3 (triangles).

This tendency was also observed in a previous work where a linear surfactant was used as the structure directing agent[63]. In that case, we observed a split in the peak of the density profiles of the surfactant heads, which was also observed in some of the systems studied here, although less significantly because of the lower inorganic concentration. If the concentration of I_2 was high enough, such a tendency would be more evident.

In Figure 12, the density profiles of the inorganic segments and the functional groups of the hybrid precursors in systems containing I_2TH (top), I_2THT (middle), and I_2THT_3 (bottom) are given.

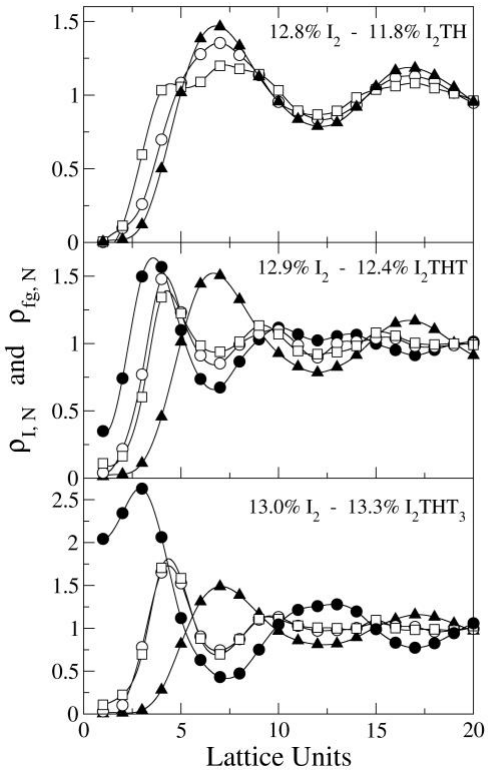

Fig. 12. Normalized density profiles of the inorganic beads (triangles), $T_\square$ groups (blank squares), terminal solvophobic groups (solid circles), and amine groups H (blank circles), in systems containing I_2TH (top), I_2THT (center), and I_2THT_3 (bottom).

In the system containing I_2TH, the functional organic group (-TH) seems to be completely included in the inorganic wall surrounding the mesopores, and little difference is observed between the density profile of the solvophilic and solvophobic groups. Although experimentally, the amine groups in materials synthesized using AP are accessible to adsorbed molecules, our simulations indicate that the functional groups will remain in the inorganic rich region and not penetrate to the core of the micelle. The difference in solvent properties of I_2 and I_2TH cause the destruction of the liquid crystal at high concentrations of I_2TH.

On the other hand, in the systems containing I_2THT or I_2THT_3, the penetration of the organic groups into the core of the cylindrical aggregates becomes evident. In particular, the density profile of the organic group -THT shows a very well defined first maximum for the solvophobic groups in the hybrid precursor, which are clearly separated from the first maximum of the inorganic density profile.

The penetration of the solvophobic groups into the core of the cylindrical micelles becomes more evident when the hybrid precursor I_2THT_3 was used. The terminal organic group, $-T_3$, deeply penetrates the core of the cylindrical micelle, while the T_α penetration is restricted to the surface of the core. This behavior is consistent with that observed in the lamellar structures.

A high concentration of the organic groups into the core of the cylindrical aggregates is preferred if the resulting mesoporous material is to be used to perform a given operation where functional groups play an important role, such as a selective adsorption or catalysis. However, if such a concentration becomes too high, the diffusion of some molecules through the mesopores may be reduced or even completely prevented. The concentration of the functional group of the hybrid precursors in the core of the aggregates varies with their chain length, and the longer this chain, the smaller the resulting pore size. In particular, at one lattice unit from the center of the cylindrical aggregates, the density of I_2THT_3 is already very high, which means that the pore diameter is not bigger than one single lattice site. Keeping in mind the approximation of the lattice model, we can say that the hybrid precursor I_2THT_3 might lead to complete pore filling, preventing any efficient molecular diffusion through the pores. Nevertheless, since the functional organic groups are not as rigid as the inorganic framework, diffusion of small molecules should be possible, but it should be expected to be considerably slower than in a non-functionalized material.

A different hybrid precursor, with a smaller functional group, reduces this effect significantly. In particular, the concentration of the functional groups of I_2THT and I_2TH at one lattice unit from the center of the cylinders is respectively seven and ten times smaller than that of the functional group of I_2THT_3. Since the concentration varies inversely with the cube of the radius, there can be a difference in the pore radius of roughly two lattice units.

Conclusions

We have shown that the transitions observed between hexagonal and disordered phases, or hexagonal and lamellar phases in co-condensation of TEOS and hybrid silica precursors in the presence of surfactant aggregates depend strongly on the nature of the hybrid functional group. In particular, if the hybrid functional group is sufficiently solvophobic, it can swell the solvophobic core of the cylindrical aggregates leading to the formation of lamellar structures. On the other hand, if the functional group is not able to swell the core of the cylindrical aggregates, the change in the interfacial properties will lead to the destruction of the ordered phases at high concentrations of the hybrid precursor.

Our models are not able to capture differences in the spacing of cylinders when adding hybrid precursors, which is probably due to the use of a simple model. Probably such details can be studied more efficiently with fully atomistic simulations of a preformed cylindrical aggregate in the presence of silica and organosilica precursors. Nevertheless, simulations using simple models can provide a useful guideline for the expected stability of a liquid crystal phase when hybrid precursors, cosolvents or cosurfactants are added to the system.

Acknowledgements

This work was supported by project CTQ2008-06469 of the Ministerio de Ciencia e Innovación, and EU funded project No. SES6-CT-2005-020133. A.P. acknowledges the support of a URV graduate student fellowship.

References

(1) Sanchez, C.; Soler-Illia, G. J. D. A.; Ribot, F.; Lalot, T.; Mayer, C. R.; Cabuil, V. *Chemistry of Materials* **2001**, *13*, 3061.

(2) Soler-illia, G. J. D.; Sanchez, C.; Lebeau, B.; Patarin, J. *Chemical Reviews* **2002**, *102*, 4093.

(3) Soler-Illia, G. J. D. A.; Crepaldi, E. L.; Grosso, D.; Sanchez, C. *Current Opinion in Colloid & Interface Science* **2003**, *8*, 109.

(4) Melero, J. A.; van Grieken, R.; Morales, G. *Chemical Reviews* **2006**, *106*, 3790.

(5) Nicole, L.; Boissiere, C.; Grosso, D.; Quach, A.; Sanchez, C. *Journal of Materials Chemistry* **2005**, *15*, 3598.

(6) Berggren, A.; Palmqvist, A. E. C.; Holmberg, K. *Soft Matter* **2005**, *1*, 219.

(7) Soler-Illia, G. J. A. A.; Innocenzi, P. *Chemistry-a European Journal* **2006**, *12*, 4478.

(8) Wan, Y.; Shi, Y. F.; Zhao, D. Y. *Chemical Communications* **2007**, 897.

(9) Wan, Y.; Zhao, D. Y. *Chemical Reviews* **2007**, *107*, 2821.

(10) Hoffmann, F.; Cornelius, M.; Morell, J.; Froba, M. *Angewandte Chemie-International Edition* **2006**, *45*, 3216.

(11) Sanchez, C.; Boissiere, C.; Grosso, D.; Laberty, C.; Nicole, L. *Chemistry of Materials* **2008**, *20*, 682.

(12) Beck, J. S.; Vartuli, J. C.; Roth, W. J.; Leonowicz, M. E.; Kresge, C. T.; Schmitt, K. D.; Chu, C. T. W.; Olson, D. H.; Sheppard, E. W.; Mccullen, S. B.; Higgins, J. B.; Schlenker, J. L. *Journal of the American Chemical Society* **1992**, *114*, 10834.

(13) Kresge, C. T.; Leonowicz, M. E.; Roth, W. J.; Vartuli, J. C.; Beck, J. S. *Nature* **1992**, *359*, 710.

(14) Huo, Q. S.; Margolese, D. I.; Ciesla, U.; Feng, P. Y.; Gier, T. E.; Sieger, P.; Leon, R.; Petroff, P. M.; Schuth, F.; Stucky, G. D. *Nature* **1994**, *368*, 317.

(15) Huo, Q. S.; Margolese, D. I.; Ciesla, U.; Demuth, D. G.; Feng, P. Y.; Gier, T. E.; Sieger, P.; Firouzi, A.; Chmelka, B. F.; Schuth, F.; Stucky, G. D. *Chemistry of Materials* **1994**, *6*, 1176.

(16) Bagshaw, S. A.; Prouzet, E.; Pinnavaia, T. J. *Science* **1995**, *269*, 1242.

(17) Zhao, D. Y.; Feng, J. L.; Huo, Q. S.; Melosh, N.; Fredrickson, G. H.; Chmelka, B. F.; Stucky, G. D. *Science* **1998**, *279*, 548.

(18) Boettcher, S. W.; Fan, J.; Tsung, C. K.; Shi, Q. H.; Stucky, G. D. *Accounts of Chemical Research* **2007**, *40*, 784.

(19) Kanatzidis, M. G. *Advanced Materials* **2007**, *19*, 1165.

(20) Asefa, T.; MacLachan, M. J.; Coombs, N.; Ozin, G. A. *Nature* **1999**, *402*, 867.

(21) Macquarrie, D. J. *Chemical Communications* **1996**, 1961.

(22) Burkett, S. L.; Sims, S. D.; Mann, S. *Chemical Communications* **1996**, 1367.

(23) Hartmann, M. *Chemistry of Materials* **2005**, *17*, 4577.

(24) Li, C. M.; Liu, J.; Shi, X.; Yang, J.; Yang, Q. H. *Journal of Physical Chemistry C* **2007**, *111*, 10948.

(25) Gao, Q.; Xu, W. J.; Xu, Y.; Wu, D.; Sun, Y. H.; Deng, F.; Shen, W. L. *Journal of Physical Chemistry B* **2008**, *112*, 2261.

(26) Mercier, L.; Pinnavaia, T. J. *Advanced Materials* **1997**, *9*, 500.

(27) Mercier, L.; Pinnavaia, T. J. *Environmental Science & Technology* **1998**, *32*, 2749.

(28) Liu, A. M.; Hidajat, K.; Kawi, S.; Zhao, D. Y. *Chemical Communications* **2000**, 1145.

(29) Brown, J.; Mercier, L.; Pinnavaia, T. J. *Chemical Communications* **1999**, 69.

(30) Bois, L.; Bonhomme, A.; Ribes, A.; Pais, B.; Raffin, G.; Tessier, F. *Colloids and Surfaces a-Physicochemical and Engineering Aspects* **2003**, *221*, 221.

(31) Yoshitake, H.; Yokoi, T.; Tatsumi, T. *Chemistry of Materials* **2003**, *15*, 1713.

(32) Jun, Y. S.; Huh, Y. S.; Park, H. S.; Thomas, A.; Jeon, S. J.; Lee, E. Z.; Won, H. J.; Hong, W. H.; Lee, S. Y.; Hong, Y. K. *Journal of Physical Chemistry C* **2007**, *111*, 13076.

(33) Brady, R.; Woonton, B.; Gee, M. L.; O'Connor, A. J. *Innovative Food Science & Emerging Technologies* **2008**, *9*, 243.

(34) Walcarius, A. *Electroanalysis* **1998**, *10*, 1217.

(35) Walcarius, A. *Electroanalysis* **2008**, *20*, 711.

(36) Sanchez, C.; Lebeau, B.; Chaput, F.; Boilot, J. P. *Advanced Materials* **2003**, *15*, 1969.

(37) Penard, A. L.; Gacoin, T.; Boilot, J. P. *Accounts of Chemical Research* **2007**, *40*, 895.

(38) Alauzun, J.; Besson, E.; Mehdi, A.; Reye, C.; Corriu, R. J. P. *Chemistry of Materials* **2008**, *20*, 503.

(39) Yokoi, T.; Yoshitake, H.; Tatsumi, T. *Journal of Materials Chemistry* **2004**, *14*, 951.

(40) Hiyoshi, N.; Yogo, K.; Yashima, T. *Chemistry Letters* **2004**, *33*, 510.

(41) Hiyoshi, N.; Yogo, K.; Yashima, T. *Microporous and Mesoporous Materials* **2005**, *84*, 357.

(42) Harlick, P. J. E.; Sayari, A. *Molecular Sieves: From Basic Research to Industrial Applications, Pts a and B* **2005**, *158*, 987.

(43) Kim, S.; Ida, J.; Guliants, V. V.; Lin, J. Y. S. *Journal of Physical Chemistry B* **2005**, *109*, 6287.

(44) Knowles, G. P.; Graham, J. V.; Delaney, S. W.; Chaffee, A. L. *Fuel Processing Technology* **2005**, *86*, 1435.

(45) Knowles, G. P.; Delaney, S. W.; Chaffee, A. L. *Industrial & Engineering Chemistry Research* **2006**, *45*, 2626.

(46) Yokoi, T.; Yoshitake, H.; Yamada, T.; Kubota, Y.; Tatsumi, T. *Journal of Materials Chemistry* **2006**, *16*, 1125.

(47) Harlick, P. J. E.; Sayari, A. *Industrial & Engineering Chemistry Research* **2006**, *45*, 3248.

(48) Harlick, P. J. E.; Sayari, A. *Industrial & Engineering Chemistry Research* **2007**, *46*, 446.

(49) Sakamoto, Y.; Nagata, K.; Yogo, K.; Yamada, K. *Microporous and Mesoporous Materials* **2007**, *101*, 303.

(50) Knofel, C.; Descarpentries, J.; Benzaouia, A.; Zelenak, V.; Mornet, S.; Llewellyn, P. L.; Hornebecq, V. *Microporous and Mesoporous Materials* **2007**, *99*, 79.

(51) Hicks, J. C.; Drese, J. H.; Fauth, D. J.; Gray, M. L.; Qi, G. G.; Jones, C. W. *Journal of the American Chemical Society* **2008**, *130*, 2902.

(52) Kumar, P.; Kim, S.; Ida, J.; Guliants, V. V. *Industrial & Engineering Chemistry Research* **2008**, *47*, 201.

(53) Hatton, B.; Landskron, K.; Whitnall, W.; Perovic, D.; Ozin, G. A. *Accounts of Chemical Research* **2005**, *38*, 305.

(54) Treuherz, B. A.; Khimyak, Y. Z. *Microporous and Mesoporous Materials* **2007**, *106*, 236.

(55) Yang, Y.; Sayari, A. *Chemistry of Materials* **2008**, *20*, 2980.

(56) Wang, X. G.; Lin, K. S. K.; Chan, J. C. C.; Cheng, S. F. *Journal of Physical Chemistry B* **2005**, *109*, 1763.

(57) Wang, X. G.; Lin, K. S. K.; Chan, J. C. C.; Cheng, S. *Chemical Communications* **2004**, 2762.

(58) Zelenak, V.; Badanicova, M.; Murafa, N.; Vannio, U., *unpublished work.*

(59) Fan, J.; Boettcher, S. W.; Tsung, C. K.; Shi, Q.; Schierhorn, M.; Stucky, G. D. *Chemistry of Materials* **2008**, *20*, 909.

(60) Siperstein, F. R.; Gubbins, K. E. *Langmuir* **2003**, *19*, 2049.

(61) Firouzi, A.; Atef, F.; Oertli, A. G.; Stucky, G. D.; Chmelka, B. F. *Journal of the American Chemical Society* **1997**, *119*, 3596.

(62) Bhattacharya, S.; Gubbins, K. E. *Journal of Chemical Physics* **2005**, *123*.

(63) Patti, A.; Mackie, A. D.; Siperstein, F. R. *Langmuir* **2007**, *23*, 6771.

(64) Patti, A.; Siperstein, F. R.; Mackie, A. D. *J. Phys. Chem. C* **2007**, *111*, 16035.

(65) Jorge, M.; Gomes, J. R. B.; Natalia, M.; Cordeiro, D. S.; Seaton, N. A. *Journal of the American Chemical Society* **2007**, *129*, 15414.

(66) Rao, N. Z.; Gelb, L. D. *Journal of Physical Chemistry B* **2004**, *108*, 12418.

(67) Schumacher, C.; Seaton, N. A. *Adsorption-Journal of the International Adsorption Society* **2005**, *11*, 643.

(68) Schumacher, C.; Gonzalez, J.; Perez-Mendoza, M.; Wright, P. A.; Seaton, N. A. *Industrial & Engineering Chemistry Research* **2006**, *45*, 5586.

(69) Schumacher, C.; Gonzalez, J.; Wright, P. A.; Seaton, N. A. *Journal of Physical Chemistry B* **2006**, *110*, 319.

(70) Bhattacharya, S.; Kieffer, J. *Journal of Physical Chemistry C* **2008**, *112*, 1764.

(71) Gov, N.; Borukhov, I.; Goldfarb, D. *Langmuir* **2006**, *22*, 605.

(72) Frenkel, D.; Smit, B. *Understanding Molecular Simulations: From Algorithms to Applications*, 2nd ed.; Academic Press: San Diego, 2001.

(73) Kleitz, F.; Blanchard, J.; Zibrowius, B.; Schuth, F.; Agren, P.; Linden, M. *Langmuir* **2002**, *18*, 4963.

(74) Mori, Y.; Pinnavaia, T. J. *Chemistry of Materials* **2001**, *13*, 2173.